Laser-produced plasma helium-like titanium Kα x-ray source and its application to Rayleigh–Taylor instability study*

Wang Rui-Rong(王瑞荣)[a)b)†], Chen Wei-Min(陈伟民)[a)], Wang Wei(王 伟)[b)], Dong Jia-Qin(董佳钦)[b)], and Xiao Sha-Li(肖沙里)[a)]

[a)] *The Key Laboratory of Optoelectronic Technology and System, Ministry of Education, Chongqing University, Chongqing* 400044, *China*
[b)] *State Key Laboratory of High Power Laser and Physics, Shanghai Institute of Laser Plasma, Shanghai* 201800, *China*

(Received 5 October 2009; revised manuscript received 11 December 2009)

Several experiments are performed on the ShenGuang-II laser facility to investigate an x-ray source and test radiography concepts. X-ray lines emitted from laser-produced plasmas are the most practical means of generating these high intensity sources. By using a time-integrated space-resolved keV spectroscope and pinhole camera, potential helium-like titanium Kα x-ray backlighting (radiography) line source is studied as a function of laser wavelength, ratio of pre-pulse intensity to main pulse intensity, and laser intensity (from 7.25 to $\sim 11.3\times10^{15}$ W/cm^2). One-dimensional radiography using a grid consisting of 5 μm Au wires on 16 μm period and the pinhole-assisted point projection is tested. The measurements show that the size of the helium-like titanium Kα source from a simple foil target is larger than 100 μm, and relative x-ray line emission conversion efficiency $\xi_{\rm x}$ from the incident laser light energy to helium-like titanium K-shell spectrum increases significantly with pre-pulse intensity increasing, increases rapidly with laser wavelength decreasing, and increases moderately with main laser intensity increasing. It is also found that a gold gird foils can reach an imaging resolution better than 5-μm featured with high contrast. It is further demonstrated that the pinhole-assisted point projection at such a level will be a novel two-dimensional imaging diagnostic technique for inertial confinement fusion experiments.

Keywords: x-ray source, plasma diagnostic techniques, x-ray spectra
PACC: 5250D, 5270, 3220R

1. Introduction

X-ray radiography is an important tool for diagnosing and imaging Rayleigh–Taylor (R–T) instability and dense materials for laser experiments. These experiments need intense and efficient multi-keV x-ray backlighting.[1−4] X-ray lines emitted from laser-produced plasmas are the most practical means of generating these high intensity sources.[5−8]

Although x-ray backlighting is a simple concept, we do not have a firm understanding or a model that predicts multi-keV x-ray source parameters[9] under experimental conditions. It has been shown in the past few years that solid targets enable the creating of multi-keV sources at various photon energies but exhibit low efficiencies.[10,11] It is believed that a pre-pulse creates a weakly ionised pre-plasma in front of the target before the arrival of the main pulse and that this pre-plasma plays an essential role in the laser–matter interaction.[12] Because low-level pre-pulses added to the plasma-creating pump laser pulse can significantly improve the output intensity of multi-keV x-ray, much attention has been paid recently to pre-pulsed multi-keV x-ray source. Therefore, the control and optimization of the x-ray emission of plasmas produced by high intensity laser–solid interaction under different pre-pulse conditions becomes a subject of current interest.

In this work we concentrate primarily on x-ray yield $\xi_{\rm x}$ for the helium (He)-like-titanium(Ti) Kα ($\sim$4.75 keV) lines as a function of pre-pulse level, laser wavelength, and laser intensity. $\xi_{\rm x}$ is defined as the x-ray photons in 4π sr per incident laser joule, generated by a laser irradiated disk target. The experimental parameters (laser intensity, and ratio of pre-pulse intensity to heating pulse intensity) are optimized in order to design the experimental configuration to achieve a maximum He-like-Ti-Kα x-ray yield. This config-

*Project supported by the National High Technology Development Program of China (Grant No. 2009AA8046006).
†Corresponding author. E-mail: wangrr59@citiz.net
© 2010 Chinese Physical Society and IOP Publishing Ltd

uration is tested on the ShenGuang II (SG-II) laser facility. In the present paper we report on the enhancement of the He-like-Ti-Kα ($\sim$4.75 keV) lines by exploding a thin foil with a laser pre-pulse. Ti x-ray emission spectra are measured with a flat crystal spectrometer (FCS). Other diagnostic instrument is a pinhole camera (PHC) that is used to measure the full width at half maximum (FWHM) of the He-like-Ti K shell x-ray source size. The primary purpose of this work is to catalogue the conversion efficiencies for various laser conditions and to describe the critical parameters affecting the backlighting line production. A second motivation for this work then is to determine the feasibility of the pinhole-assisted point projection (PAPP).

2. Experimental setup

The experiment was performed on the SG-II laser facility. Figure 1 gives a schematic view of the experimental chamber. The planar solid target of titanium (Z = 22, 5-μm-thick foil) were illuminated by Nd-glass high power laser with either double frequency ($\lambda_{\rm L}$ = 0.53 μm) or triple frequency ($\lambda_{\rm L}$ = 0.35 μm), pulse-width $T_{\rm L}$ = 80 ps, and different intensities. The x-ray measurements reported herein were performed with an x-ray flat crystal spectrograph that had been described by Wang *et al.*[13] For the He-like-Ti K-shell radiation, a Bragg diffraction crystal (pentaerythritol-tetrakis (PET) (002, 2d of 0.876 nm)) was utilised. A 40-μm-thick Ti foil was used to eliminate the visible light and further filter the He-like-Ti K-shell radiation. Imaging plate (IP) was used as an x-ray recording element. The spectrograph was mounted in the target chamber at an angle of approximately 30° with respect to the target normal. The pinhole camera was rotated 40° relative to the incident laser beam. On the assumption that the plasma was optically thin, this geometry would have little difference in measured yield as a function of observation angle. The Ti target was exposed to the amplified spontaneous emission (ASE) and the pre-pulse at different laser intensity contrasts in a few nanoseconds prior to the main pulse. We adopted a one-side irradiation scheme with cone angles above 41° from the target normal as indicated in Fig. 1. The four beams pointed to the centre of the target located in the chamber centre. The effects of the pre-pulses having different laser intensity contrast ratios, and the incident laser wavelengths (0.53 and 0.35 μm) were studied to compare with the results obtained from our analytical model giving the conversion efficiencies (CEs) as a function of atomic number and electron temperature.

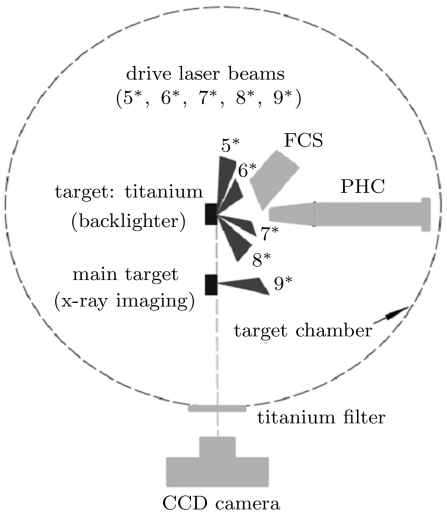


Fig. 1. Laser beams and diagnostics configuration, where FCS stands for flat crystal spectrograph, and PHC for pinhole camera, with visible lighter eliminated by a titanium filter.

Table 1 summarises the experimental parameters for each shot. In a first series of experiments composed

Table 1. Summary of the laser shot series with a 5 μm-thick titanium foil, and laser conditions (energies at 3ω and laser intensities at the initial surface of the foil).

shot number	delay /ns	pre-pulse energy/J	heating pulse energy/J	pre-pulse laser intensity/$\times 10^{15}$W$\cdot$cm^{-2}	heating pulse laser intensity/$\times 10^{15}$W$\cdot$cm^{-2}
110703	2.02	6.84	113.94	0.458	7.63
111004	2.02	114.72	168.51	7.69	11.29
111007	3.04	86.66	163.97	5.806	10.99
111102	2.02	6.17	108.25	0.41	7.25
111208	2.02	22.23	123.02	1.49	8.24
111210	2.03	31.74	158.9	2.13	10.64
111505	2.02	3.47	121.12	0.23	8.115
111507	2.02	3.02	112.6	0.20	7.54

of eight shots, the pre-pulse energy was in a range from 3 to ∼115 J and the main pulse average energy was 33 J/ beam for the heating pulse with a spot diameter of 100 μm. The total laser intensities are also shown in Table 1 for each pulse. Taking into account the angles of the beams incident on the target under the assumption of uniform irradiation over a focal spot, the total intensity could be roughly evaluated from the beam aperture. The real intensity profile was not measured in the actual conditions of these experiments.

3. Experimental results

3.1. He-like Ti x-ray source spot size and conversion efficiency measurement

Two instruments were used to characterise the He-like-Ti K shell x-ray source.[14] The x-ray emission volume was observed by time-integrating PHC. The PHC has a front side view at a ∼10° angle with respect to the target normal. The magnification is 3× and a 20 μm-thick titanium filter eliminated the visible light and restricted the energy above 5 keV. IP was used as an x-ray recording element. The PHC images in Fig. 2 show that the hard x-rays emission size increases when the foil is exploded by the pre-pulse compared with the case without applying a pre-pulse.

The required spatial resolution for diagnosing and imaging R–T instability and dense material experiments is better than 10 μm. If we intend to perform point projection imaging, we will need an x-ray source smaller than 10 μm in size. Our measurements performed at the SG-II, however, show that the typical He-like-Ti Kα source size is around 160 μm even though the actual laser spot size is < 100 μm. Figure 3 shows a pinhole image of the about 4.75 keV He-like-Ti K shell source from the SG-II laser facility where the measured FWHM of the x-ray spot size is ∼154 μm. The x-ray spot sizes are still larger than the laser spot size of < 100 μm, owing to the large spreading of the relativistic electrons. As demonstrated in the PHC images, this emission zone size is clearly increased in the case of plasma expansion. The size increase, the higher intensity, and the longer emission duration demonstrate that the CE is enhanced by a pre-pulse.

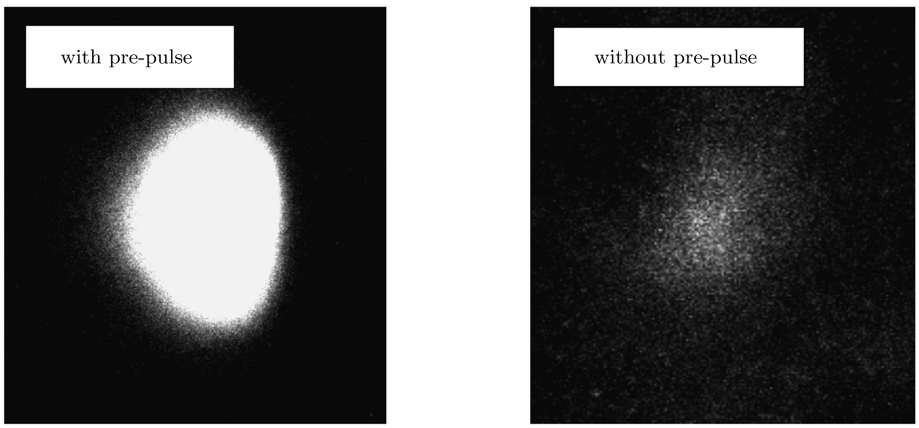


Fig. 2. X-ray pinhole camera images, showing a comparison of compare the pre-pulse effect for the front side at view angle of 10° with respect to the foil normal at $I_{\rm L} \approx 1.3 \times 10^{15}$ W·cm^{-2} between shot No. 111501 (with applying a pre-pulse) and shot No. 102501 (without applying a pre-pulse). The laser beam is incident from left to right.

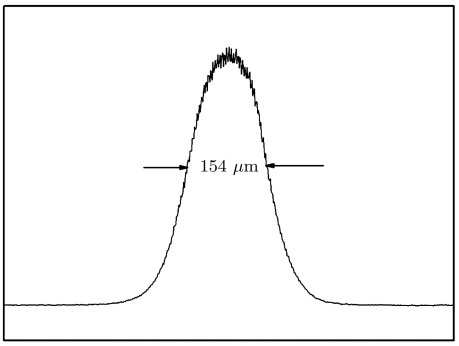


Fig. 3. Azimuthally averaged line profile from with pre-pulse in Fig. 2.

The FCS is configured to find the high-energy part of the spectrum (4.7–4.9 keV), covering the He-like and hydrogen (H)-like Ti line spectral regions. The observed spectral region goes from 2 to 2.8 Å (1 Å = 0.1 nm) (4.43 keV–6.2 keV). The spectral range was

adjusted by choosing appropriate filter materials. Figure 4 illustrates the lines considered in these measurements. Note that in each spectrum there is an energy limit over which the photon yield is integrated. In all cases this includes the bulk of the line emission that could be useful for a relatively narrow energy band (ΔE) x-ray imaging device ($\Delta E/E \sim 0.1 \sim 0.2$). In particular, this includes the He-like resonance and intercombination ($2^1P_1, 2^3P_1 \rightarrow 1^1S_0$) transitions and Li-like satellite lines of Ti (∼4.7 keV). We also observed the 'cold' Kα line. This line represents the emission from the decay of an atom which is not ionised in the L shell but excited by electron impact taking place somewhere in the colder regions of the disk target (i.e. beyond the ablated plasma). This ionisation mechanism works most efficiently for electrons having energies at least 3 times greater than the ionisation potential of the K shell, thus only relatively energetic electrons are responsible for this type of excitation. As a result, the Kα line is usually observed only when a significant number of hot electrons are produced, we have found that the production efficiency of the Kα line is significantly less than that of lines produced in the thermal plasma (such as the more common Li-, He-, and H-like transitions). From the result, we estimate the conversion efficiency from the laser energy to He-like-Ti K shell photons for the planar Ti target. But we still need to understand laser coupling efficiency, hot electron conversion efficiency, and radiation transport originating from all these different shapes. If laser irradiance at $\lambda_{\rm L} = 0.35$ μm increases the local temperature compared with that at $\lambda_{\rm L} = 0.53$ μm, then the line production efficiency can be expected to be enhanced because of the larger plasma densities produced at short wavelength laser. Thus the maximum high energy line emission will occur from the highest density and temperature region available in the plasma. The size of this region naturally depends on laser irradiance condition and details of the laser light absorption and energy transport mechanisms. We now search for the options to create more efficient laser-driven conditions.

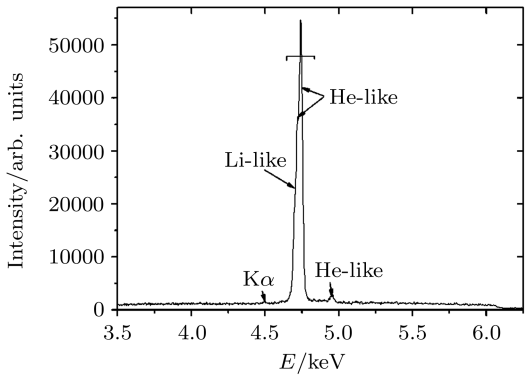


Fig. 4. Shot No. 111501 Ti K shell x-ray spectrum from a laser irradiated disk. Bracket-indicated spectral region is the region over which x-ray yield is integrated.

In addition, the peak of this spectrum is then assigned to the 4.75 keV He-like-Ti Kα emission energy as illustrated in Fig. 4. Each spectrum is composed of the bremsstrahlung continuous emission and the characteristic spectrum. In all cases it includes the image Bremsstrahlung background. Therefore, when the number of He-like-Ti Kα photons is deduced by integrating this line, the image Bremsstrahlung background must be subtracted from it. At present the x-ray photon number is only roughly assessed in that the conversion from optical density to intensity cannot be still absolutely calibrated. The relative photon number is obtained by only taking into account filter transmission, and the slid angle subtended by the analysed area of the IP. In Table 2 we summarise the results from individual laser shots to demonstrate the variation in conversion efficiency $\xi_{\rm x}$, with laser intensity, pre-pulse/heating pulse intensity ratio, and wavelength for He-like-Ti K shell x-ray resonance transitions. The Ti data show that the He-like-Ti Kα x-ray yield is greatly improved when the ratio of pre-pulse intensity to main pulse intensity is increased. Moreover, a dramatic increase relative to data at $\lambda_{\rm L} = 0.53$ μm is observed at a short wavelength ($\lambda_{\rm L} = 0.35$ μm). Remarkable improvements in x-ray line conversion efficiency are observed for He-like-Ti Kα x-ray lines when irradiation from a $\lambda_{\rm L} = 0.35$ μm laser (for fixed $I_{\rm L}$) is used.

Table 2. Line conversion efficiency $\xi_{\rm x}$ for Ti K shell x-ray as a function of laser wavelength, and ratio of pre-pulse intensity to heating pulse intensity.

pre-pulse laser intensity/$\times 10^{15}$W$\cdot$cm^{-2}	heating pulse laser intensity/$\times 10^{15}$W$\cdot$cm^{-2}	delay/ns	laser wavelength /μm	laser pulse /ps	$\xi_{\rm x}$ (x-ray photons per incident laser Joule $\times 10^{13}$)
0.20	7.54	2.02	0.35	80	0.036
0.20	7.95	2.02	0.35	80	0.058

Table 2 *contiuned*

pre-pulse laser intensity/$\times 10^{15}$W$\cdot$cm^{-2}	heating pulse laser intensity/$\times 10^{15}$W$\cdot$cm^{-2}	delay/ns	laser wavelength /μm	laser pulse /ps	ξ_x (x-ray photons per incident laser Joule $\times$ 10^{13})
0.23	8.12	2.02	0.35	80	0.067
0.31	7.27	2.02	0.35	80	0.074
0.39	8.01	2.02	0.35	80	0.073
0.46	7.63	2.02	0.35	80	0.075
0.41	7.25	2.02	0.35	80	0.072
1.49	8.24	2.02	0.35	80	0.108
2.13	10.64	2.02	0.35	80	0.110
4.08	10.80	2.02	0.35	80	0.116
5.81	10.99	2.02	0.35	80	0.120
7.69	11.29	2.02	0.35	80	0.129
0.18	7.26	2.02	0.53	80	0.008
1.95	8.76	2.02	0.53	80	0.010

3.2. Application of the He-like-Ti Kα source

The spot size of x-ray emitted from a large disk foil irradiated by a well-focused laser is too large to be used for point projection radiography. On the other hand, our current experimental setup cannot exclude the higher energy Bremsstrahlung background, and the source under measurement is a broadband source. A higher spatial resolution can be achieved if the x-ray radiation is restricted within a small volume whose size is smaller than our desired spatial resolution. The pinhole may be easily introduced between the object and the source to form a pinhole-assisted point projection (PAPP). The PAPP backlight scheme is a newly developed diagnostic technique for laser-plasma experiments, playing an important role in diagnostic experiments of inertial confinement fusion physics. As a first attempt, we tested a one-dimensional (1D) radiography concept in which a planar solid Ti foil is used as a laser target and a commercial gold grid serves as the radiography object. Our backlight imaging experiment was performed with a grid consisting of 5 μm Au wires of a 16 μm period on SG-II laser facility, and the imaging detector was a charge-coupled device (CCD) camera. The obtained image is shown in Fig. 5. For the 1D analysis the intensity values are averaged along the slit direction; the obtained line profile is shown on the right-hand side of the image. From these data we find that on the whole, the map has a good quality, and in local regions it achieves a spatial resolution better than 5-μm.

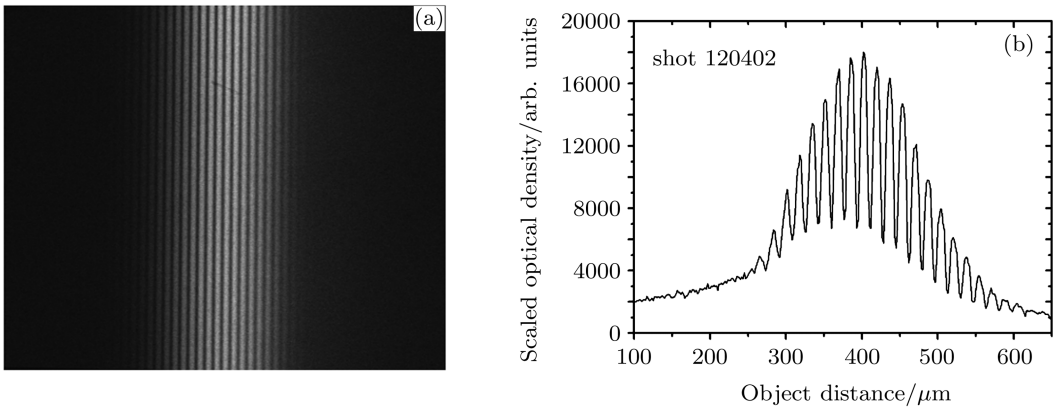


Fig. 5. Radiography of 16-μm period gold resolution gird using He-like Ti 4.75 keV source: (a) An actual radiograph, and (b) a line profile obtained by averaging the intensity values along the vertical direction (200 pixels in (a)). The 16-μm period features are clearly seen.

In addition, in our R–T experiments we also studied instability growth modes[15,16] by machining sinusoidal undulations. The R–T growth factor in laser-irradiated targets was measured by using side-on backlighting as shown in Fig. 1. The PAPP imager with a back-lighter energy of 4.75 keV was used to obtain the profile of the interface growth. It is interesting to compare the evolutions of bubbles with different shapes. Therefore, we fabricated precise perturbations on the outer surface of the target to seed R–T growth modes of interest. Machining sinusoidal undulation growths of 30, 50, and 75 μm wavelength perturbations have been observed with peak-to-valley amplitudes of 2 to 18 μm. Figure 6 shows a CCD camera image from the target with sine-wave perturbation of 75 μm wavelength, and an inscribed initial peak-to-valley amplitude of 11.45 μm. Several interesting features should be noted. As the sine-wave imploded, the outer surface became R–T unstable (dark region of the outer surface). The growth of the bubble and spike is consistent with the theoretical prediction.[17]

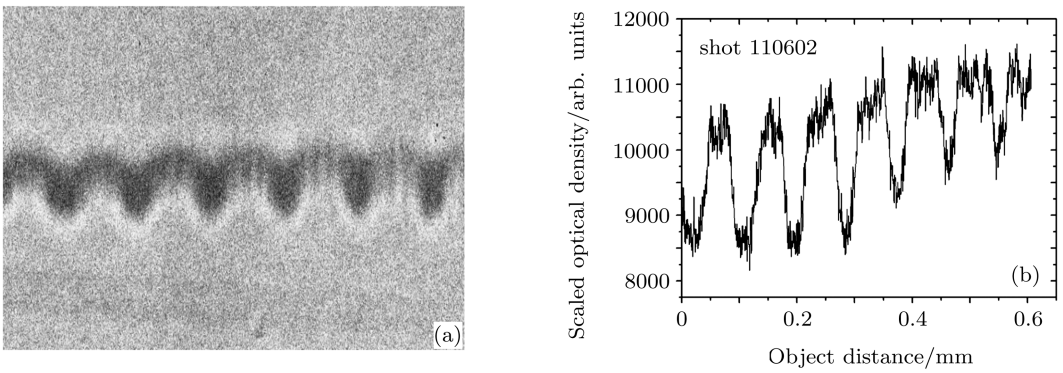


Fig. 6. Implosion of the 30 μm thick planar Al target with initial perturbation amplitude $A = 11.45$ μm. (a) An actual radio graph, and (b) a line profile obtained by averaging the intensity values vertically over the region illustrated by the horizontal curves in (a).

4. Conclusion

The conversion efficiencies from laser light into x-ray photons are measured as a function of pre-pulse level, laser wavelength, and laser intensity under a variety of laser ir-radiance conditions. These measurements show that the high-energy He-like-Ti Kα source size ($\sim$160 μm) is larger than the laser spot size ($\sim$100 μm). For He-like-Ti K shell x-ray emission we find that $\xi_{\rm x}$ decreases with photon energy increasing, moderately increases with laser intensity increasing (with $h\gamma$ fixed), increases rapidly with the increase of the ratio of pre-pulse intensity to main pulse intensity, (with $I_{\rm L}$ and $\lambda_{\rm L}$ fixed), and significantly increases with laser wavelength increasing (with $I_{\rm L}$ fixed). As a demonstration, the spatial resolution of the PAPP images is 5-μm as measured from a gold gird. This result implies that the PAPP at such a level will be a novel two-dimensional imaging diagnostic technique for inertial confinement fusion experiments.

References

[1] Bullock A B, Landen O L and Bradley D K 2001 *Rev. Sci. Instrum.* **72** 686

[2] Workman J, Fincke J R, Keiter P, Kyrala G A, Pierce T, Sublett S, Knauer J P, Robey H, Blue B, Slendinning S G and Landen O L 2004 *Rev. Sci. Instrum.* **75** 3915

[3] Riley D, Woolsey N C and Mcsherry D 2002 *Plasma Sources Sci. Technol.* **11** 484

[4] Wang J, Zhao Z Q, Cai D F, Huang W Z, He Y L and Gu Y Q 2009 *Acta Phys. Sin.* **58** 7074 (in Chinese)

[5] Boschetto D, Mourou G, Rousse A, Mordovanakis A, Hou B, Nees J, Kumah D and Clarke R 2007 *Appl Phys. Lett.* **90** 011106

[6] Huang W Z, Li Y T, Xiong Y, Zhang S G, Wen X L, Hong W, Gu Y Q, Wen T S and He Y L 2008 *Acta Phys. Sin* **57** 111 (in Chinese)

[7] Yang Z H, Song Z Y, Cui Y, Zhang H Q, Ruan F F, Shao

J X, Du J, Liu Y W, Zhu K X, Zhang X A, Shao C J, Lu R C, Yu D Y, Chen X M and Cai X H 2008 *Acta Phys. Sin.* **57** 803 (in Chinese)

[8] Matthews D L, Campbell E M, Ceglio N M, Hermes G, Kauffman R, Koppel L, Lee R, Manes K, Rupert V, Slivinsky V W, Turner R and Ze F 1983 *J. Appl. Phys.* **54** 4260

[9] Qi L H, Li Z F, Ni Q L and Chen B 2005 *Opt. Precision Eng.* **13** 272 (in Chinese)

[10] Xie L H and Zhu S F 2008 *Acta Opt. Sin.* **28** 392 (in Chinese)

[11] Workman J and Kyrala G 2001 *Proc. SPIE* **4504** 168

[12] Fill E E, Li Y, Schlogl D, Steingruber J and Nilsen J 1995 *Opt. Lett.* **20** 374

[13] Wang R R, Wang W, Wang C, Dong J Q, Sun J R and Wan B G 2003 *Acta Phys. Sin.* **52** 556 (in Chinese)

[14] Wang R R, Chen W M, Mao C S, Dong J Q and Fu S Z 2009 *Chin. Opt. Lett.* **7** 156 (in Chinese)

[15] Troussel Ph, Meyer B, Reverdin R, Angelier B and Lidove G 2005 *Rev. Sci. Instrum.* **76** 063707-1

[16] Hiroyuki S, Hiroshi A, Mitsuo N, Keisuke S, Masaharu N, Tatsuhiro S, Shinsuke F, Yohei T and Tatsuhiko Y 2003 *Rev. Sci. Instrum.* **74** 2194

[17] Wang L L and Chun L J 2003 *High Power and Particle Beams* **15** 1195 (in Chinese)